Supporting Information

Emerging Linearity Activity Trend in Oxygen Evolution Reaction with Dual-active-sites Mechanism

Li Yang,[ab†] Yuxuan Wu,[a†] Fan Wu,[a] Yuan Zhao,[b] Zhiwen Zhuo,[b] Zhaowu Wang,[c] Xiyu Li,*[b] Yi Luo,[b] Jun Jiang[b]

[a]Institutes of Physical Science and Information Technology, Anhui University, Hefei, Anhui 230601, P. R. China

[b]Hefei National Laboratory for Physical Sciences at the Microscale, CAS Center for Excellence in Nanoscience, School of Chemistry and Materials Science, University of Science and Technology of China, Hefei, Anhui 230026, P. R. China

[c]School of Physics and Engineering, Henan University of Science and Technology, Henan Key Laboratory of Photoelectric Energy Storage Materials and Applications, Luoyang, Henan 471023, P. R. China

Corresponding Author: xylizy@ustc.edu.cn

Computational Methods

The computational approach was carried out within the spin-polarized density functional theory (DFT)[1] by using the Vienna ab initio Simulation Package (VASP) package. The electronic exchange and correlation effects were simulated by the Perdew, Burke and Ernzerhof (PBE) parameterization as implemented in the generalized gradient approximation (GGA).[2] The interactions between the ion cores and valance electrons were described by the projector augmented wave (PAW) pseudo-potentials.[3] With all atoms relaxed, the convergence threshold for the max energy change and forces was set to be 10^{-4} eV and 0.02 eV/Å, respectively. The kinetic energy cutoff of 450 eV was adopted for the plane-wave expansion. As to the nanotube material, we inserted a vacuum space of 15 Å along the x and y directions for isolation, and the nanotube structure is along z axis. The K-point sampling of the Brillouin zone was set to be $1 \times 1 \times 3$ grid by using the Monkhorst-Pack scheme. Long-range van der Waals (vdW) interactions were considered in the whole calculations by employing the Grimme's DFT-D2 correction.[4] The transition states were calculated by the HOWTOs program as implemented in SSW package, we also examined the transition states through the climbing image nudged elastic band (CI-NEB) method.[5]

It is known that the oxygen molecule with high-spin ground state is often poorly described in DFT calculations. Thus, to avoid the uncertainty of PBE in computing O_2 molecule, the free energy of O_2 is derived from G_{O2} (g) = $2G_{H2O}$ (l) $- 2G_{H2}$ (g) + 4 .92 (eV) based on the whole energy change of {O_2 (g) + 4[H^+(aq) + e^-] $\rightarrow$ $2H_2O$ (l) $\rightleftharpoons$ $2H_2O$ (g)}. This treatment is adopted in the simulations of OER pathway, including the O_2 formation step (*O + *O $\rightarrow$ 2* + O_2, Eq.5, ΔG_5).
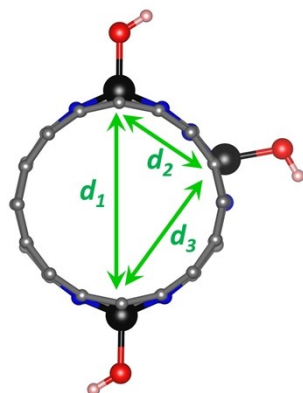
Fig. S1 Scheme of dual-active-sites with different arrangements of two single-active-sites on carbon nanotube.

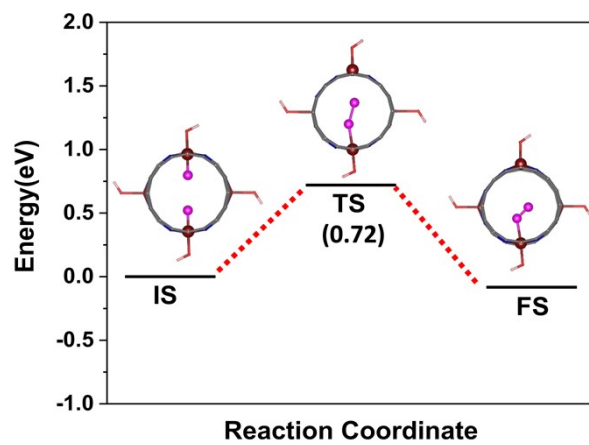**Fig. S2** Potential energy profile of the oxygen molecule formation catalyzed by the dual-active-sites $FeN_4(OH)@CNT$.

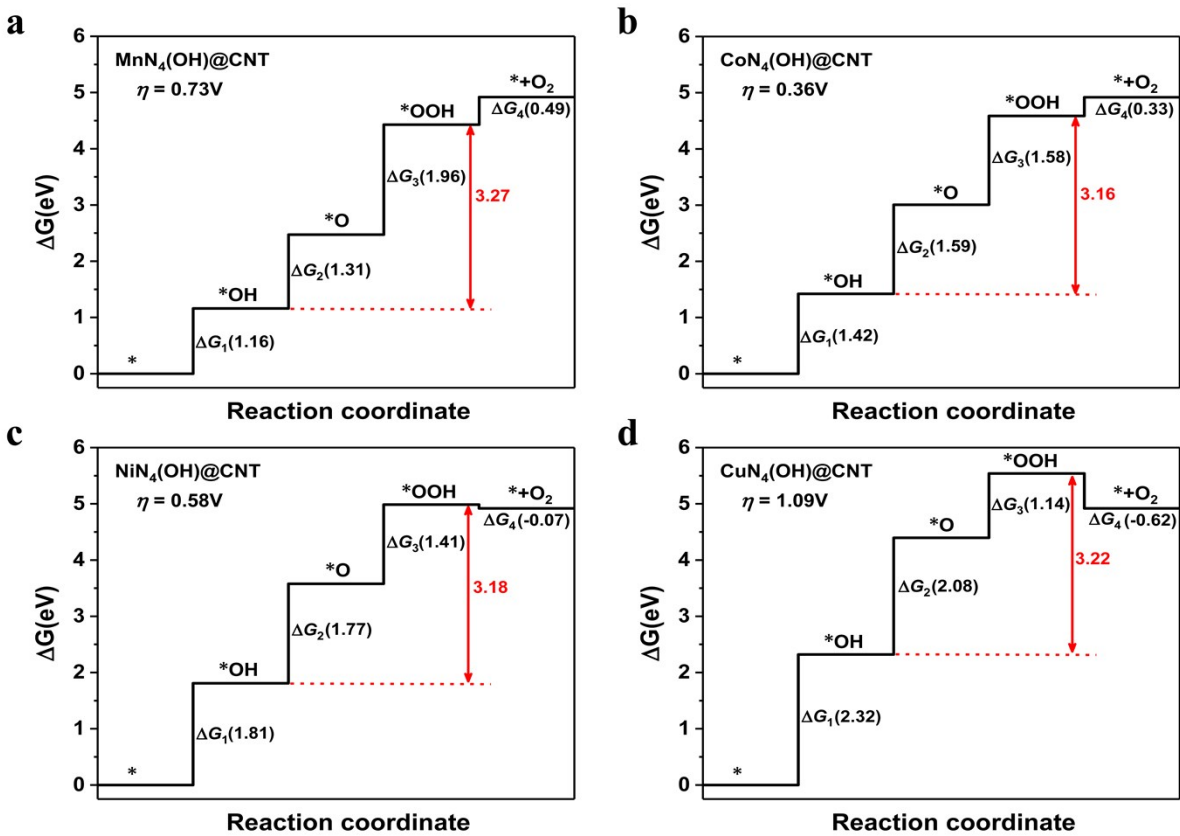**Fig. S3** Gibbs free energy diagrams of the single-active-site OER catalysis on MnN$_4$(OH)@CNT (a), CoN$_4$(OH)@CNT (b), NiN$_4$(OH)@CNT (c) and CuN$_4$(OH)@CNT (d) structures.

5

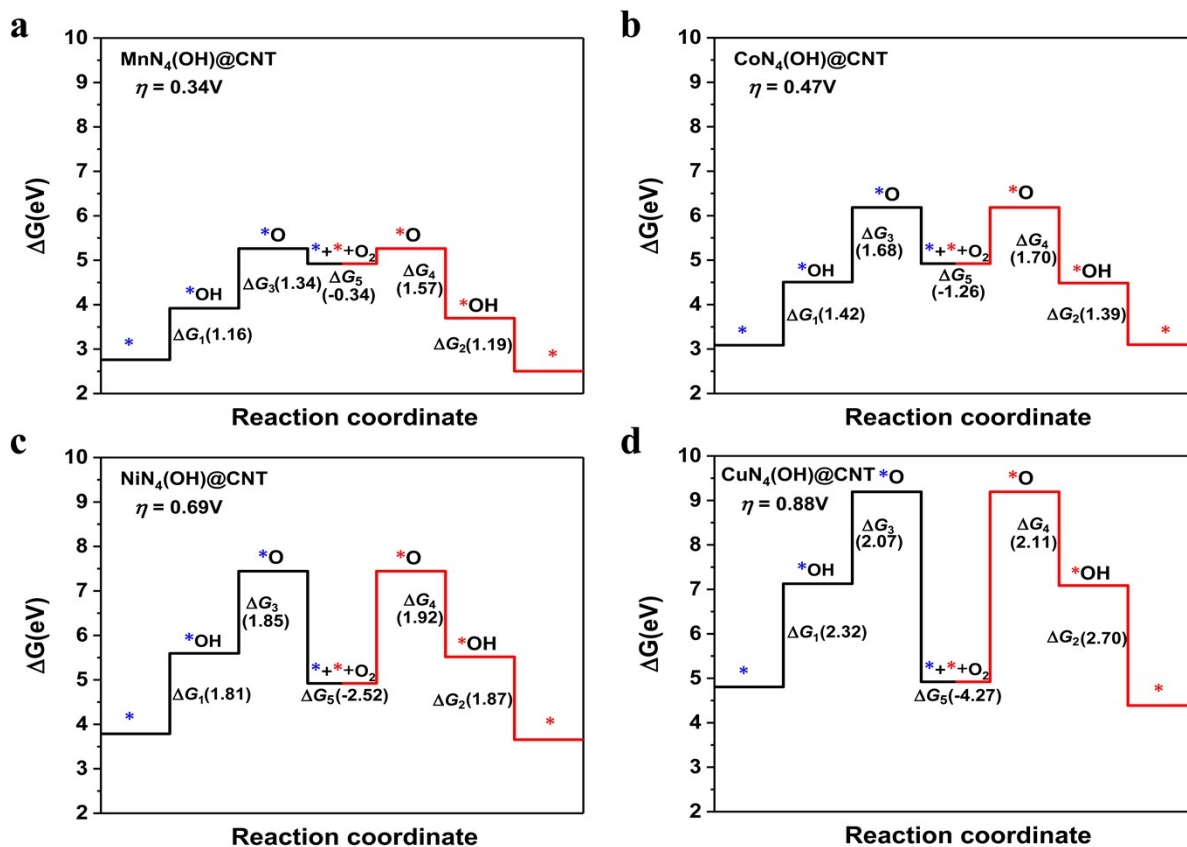**Fig. S4** Gibbs free energy diagrams following the Eq.1-5 for the dual-active-sites OER catalysis on $MnN_4(OH)@CNT$ (a), $CoN_4(OH)@CNT$ (b), $NiN_4(OH)@CNT$ (c) and $CuN_4(OH)@CNT$ (d) structures.
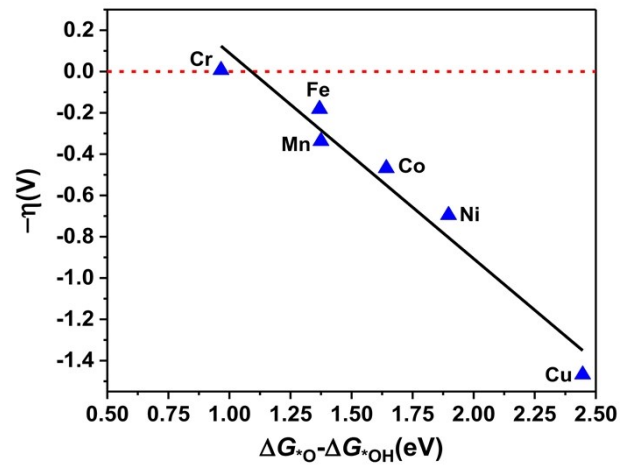
Fig. S5 The linear scaling relationship between ΔG_{*O}-ΔG_{*OH} and theoretical overpotential for OER catalysis on the dual-active-sites $TMN_4(OH)@CNT$.
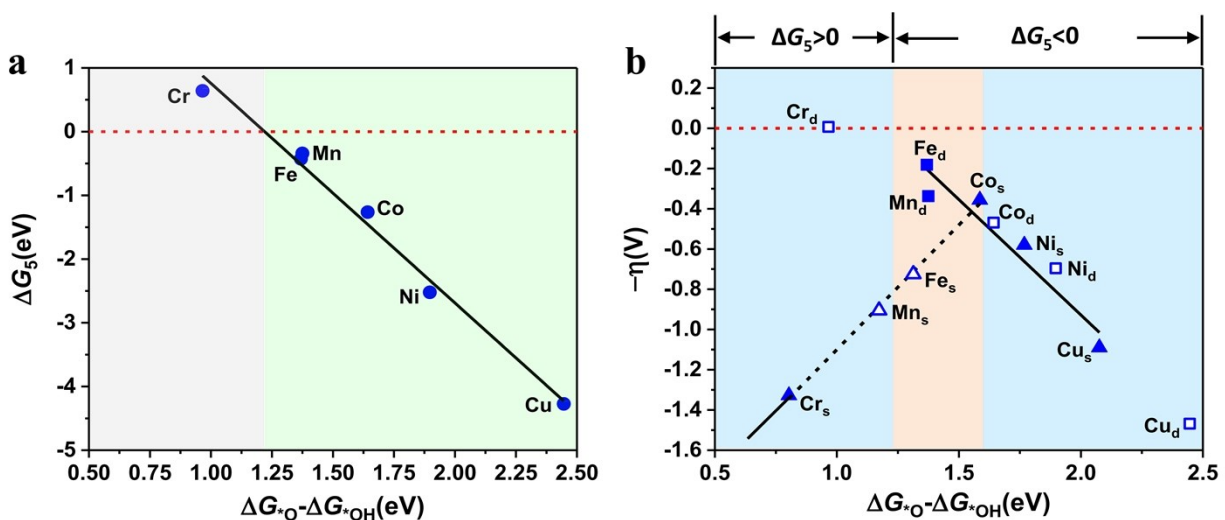
Fig. S6 The linear scaling relations between ΔG_5 and ΔG_{*O}-ΔG_{*OH} for dual-active-sites catalysis of TMN$_4$(OH)@CNT. The fitting correlational relationship is ΔG_5 = -3.45(ΔG_{*O}-ΔG_{*OH}) + 4.21. (b) The volcano scaling relations of theoretical overpotentials function with ΔG_{*O}-ΔG_{*OH} for the TMN$_4$(OH)@CNT single/dual-active-sites OER catalysis. TM$_s$ = TMN$_4$(OH)@CNT with single-active-site mechanism, TM$_d$ = TMN$_4$(OH)@CNT with dual-active-sites catalysis. The solid scatters mean the overpotentials with prior OER mechanism.
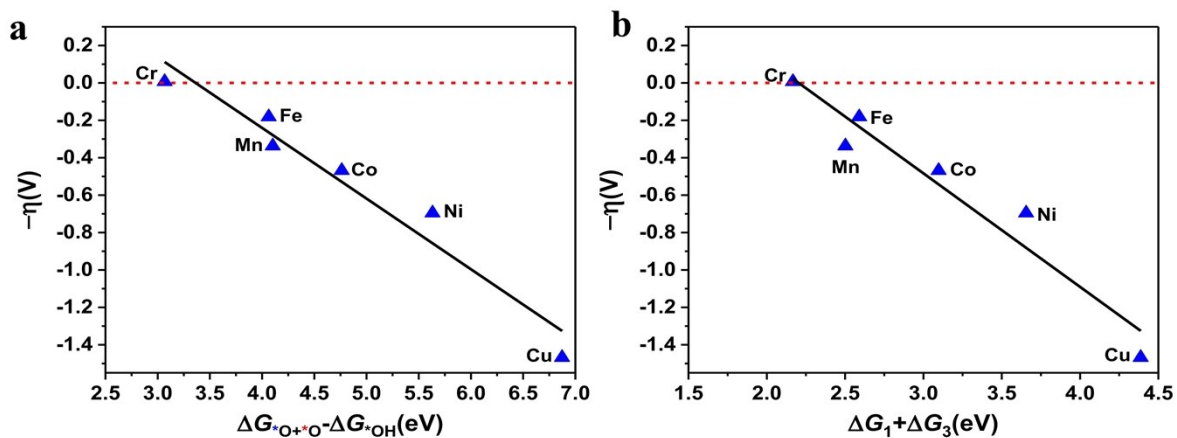
Fig. S7 Linear scaling relation of theoretical overpotential function with $\Delta G_{*O+*O} - \Delta G_{*OH}$ (a) and $\Delta G_1 + \Delta G_3$ for the TMN$_4$(OH)@CNT dual-active-sites OER catalysis.
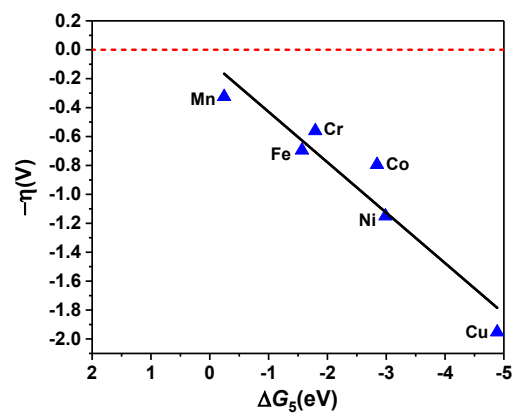
Fig. S8 Linear scaling relation of theoretical overpotentials function with ΔG_5 for the TMN$_4$(O)@CNT dual-active-sites OER catalysis.
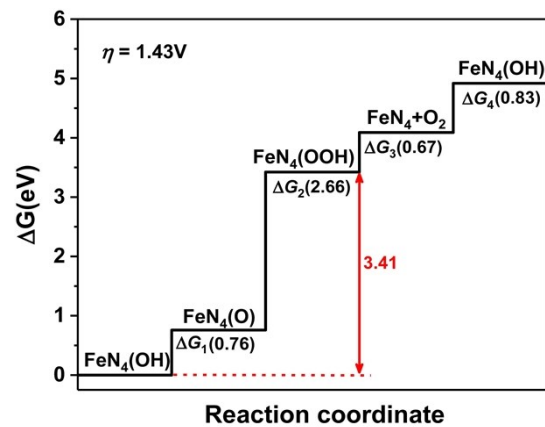
Fig. S9 Gibbs free energy diagram of the single-active-site OER catalysis at the outside of FeN$_4$(OH)@CNT with the coordinated OH involved.
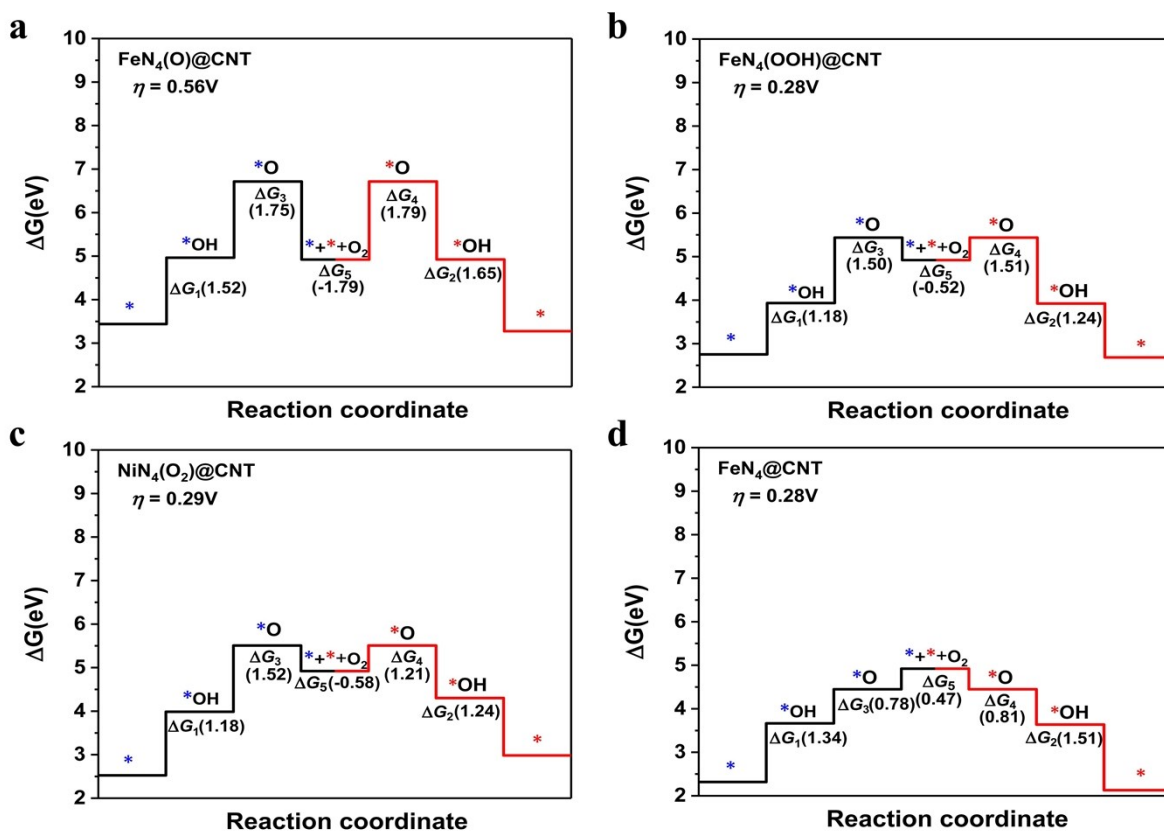
Fig. S10 Gibbs free energy diagrams following the Eq. 1-5 for the dual-active-sites OER catalysis on FeN$_4$(O)@CNT (a), FeN$_4$(OOH)@CNT (b), FeN$_4$(O$_2$)@CNT (c) and FeN$_4$@CNT (d) structures.

Fig. S11 Gibbs free energy diagrams following the Eq.1-5 for the hetero-dual-active-sites OER catalysis on $CrN_4(OH)$-$CoN_4(OH)$@CNT. The blue and red asterisk stand for the $CrN_4(OH)$ and $CoN_4(OH)$ active sites, respectively.

Fig. S12 Gibbs free energy diagrams for the dual-active-sites and single-active-site OER catalysis on $FeN_4(OH)@CNTs$ (n,0) (n= 5, 6, 7, 8, 9, 10, 11, 12) with different diameters.

14

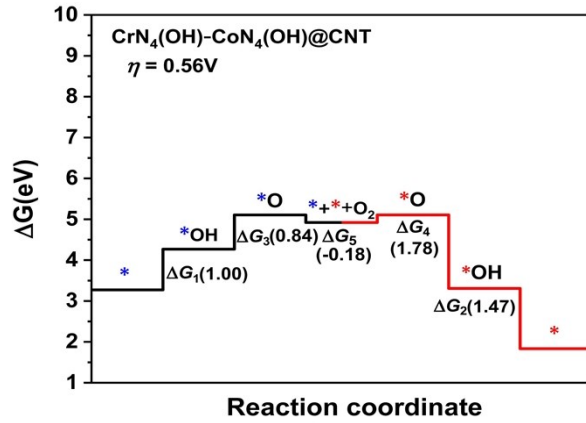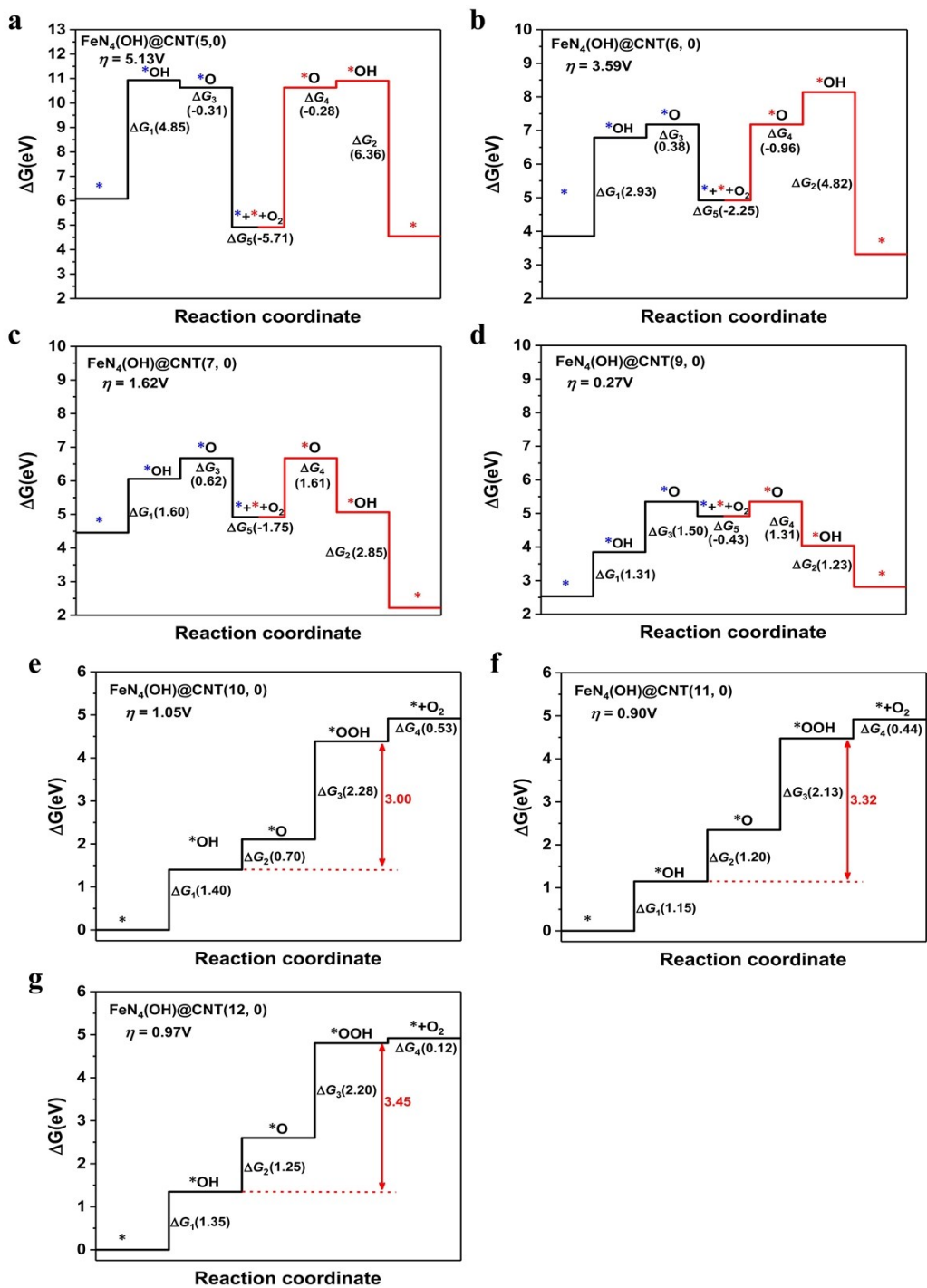The structure of CNT (4, 0) is not stable enough that even an oxygen atom adsorption could destroy its structure. As listed in Table S3, for the CNT (n, 0) (n=5, 6, 7), the weak binding energies of intermediates lead to poor OER activities in single-active-site and dual-active-sites catalysis. While as to CNT (9, 0), the d_{*O-*O} of 3.56 Å and ΔG_{*O} of 2.53 eV enable the O_2 generation from Eq.5 with effective dual-active-sites catalytic activity (η = 0.27 V). The distances between two adsorbed oxygen atoms in CNT (10, 0) and CNT (11, 0) are too far apart away from each other with d_{*O-*O} of 4.63 Å and 4.85 Å, respectively, which leads that Eq.5 cannot be realized in the cases of CNT (10, 0) and CNT (11, 0). Notably, the hydrogen bond interactions between the intermediates separately adsorbed on the two single-active-sites would be mainly determined by the distance between these two single-active-sites (inherited from the CNT diameter). For instance, the weak hydrogen bonds can generate by the two adsorbed *OOHs with the distance of ~1.71 Å and 1.93 Å, causing large overpotentials of 1.05 V and 0.90 V for CNT (10, 0) and CNT (11, 0), respectively (d=7.83 Å and 8.61 Å). When the calibre of nanotube is enlarged to CNT (12, 0) (d=9.39 Å), it can be totally treated as the scene of two isolated single-active-sites with the overpotential of 0.97 V.

Table S1 Calculated adsorption free energies for *OH (ΔG_{*OH}) on the TMN$_4$(OH) single-active-site using PBE and PBE+U. The U-J is the effective Hubbard-U parameter.

	PBE	U-J=1	U-J=2	U-J=3	U-J=4
ΔG_{*OH}(eV)	1.28	1.80	2.15	2.46	2.77

Table S2 The theoretical overpotentials (η) for OER catalysis on the single-active-site and dual-active-sites TMN$_4$(OH)@CNT.

	η(V)	
	Single-active-site Mechanism	Dual-active-sites Mechanism
CrN4(OH)	1.13	-0.01
MnN4(OH)	0.73	0.34
FeN4(OH)	0.91	0.18
CoN4(OH)	0.36	0.47
NiN4(OH)	0.58	0.69
CuN4(OH)	1.09	1.46

Table S3 The spin states of metal atoms for the structures involved in the OER pathway on the single-active-site TMN$_4$(OH)@CNT calculated by the DFT method.

	*	*OH	*O	*OOH
Cr	2.64	2.28	0.77	2.40
Mn	3.28	2.36	1.32	2.27
Fe	2.34	1.01	1.28	0.92
Co	2.61	0.17	0.55	0.10
Ni	1.54	0.68	0.92	0.70
Cu	0.47	0.09	0.13	0.12

Table S4 The spin states of metal atoms for the structures involved in the OER pathway on the dual-active-sites $TMN_4(OH)@CNT$ calculated by the DFT method.

	-	*OH-*	*OH-*OH	*O-*OH	*O-*O
Cr	2.64/2.64	2.28/2.60	2.22/2.22	1.15/2.00	0.80/0.80
Mn	3.28/3.28	2.36/3.28	2.38/2.38	1.92/2.28	1.00/1.00
Fe	2.34/2.34	1.01/2.34	1.03/1.03	1.26/1.10	1.16/1.16
Co	2.61/2.61	0.17/2.58	0.22/0.22	0.54/0.25	0.61/0.61
Ni	1.54/1.54	0.68/1.54	0.69/0.69	0.51/0.69	0.93/0.93
Cu	0.47/0.47	0.09/0.48	0.09/0.09	0.04/0.18	0.12/0.12

Table S5 The spin states of metal atoms for the structures involved in the OER pathway on the single-active-site $TMN_4(OH)@CNT$ calculated by the DFT+U method. U value of each transition metal atom was adopted according to the previous literature.[6]

	*	*OH	*O	*OOH
Cr	2.95	2.84	2.11	2.88
Mn	4.45	3.75	2.71	2.98
Fe	3.83	3.02	1.48	0.95
Co	2.65	0.01	0.38	0.01
Ni	1.63	0.92	0.96	0.95
Cu	0.59	0.004	0.016	0.04

Table S6 The spin states of metal atoms for the structures involved in the OER pathway on the dual-active-sites $TMN_4(OH)$@CNT calculated by the DFT+U method. U value of each transition metal atom was adopted according to the previous literature.[6]

	-	*OH-*	*OH-*OH	*O-*OH	*O-*O
Cr	2.95/2.95	2.84/2.94	2.80/2.80	2.22/2.64	2.03/2.03
Mn	4.45/4.45	3.75/4.45	3.72/3.72	2.71/2.79	2.70/2.70
Fe	3.83/3.83	3.02/3.88	2.95/2.95	1.50/2.93	1.44/1.44
Co	2.65/2.65	0.01/2.65	1.85/1.85	2.09/0.01	2.06/2.06
Ni	1.63/1.63	0.92/1.63	0.91/0.91	0.96/0.92	0.97/0.96
Cu	0.59/0.59	0.004/ 0.59	0.006/ 0.007	0.015/ 0.03	0.001/ 0.003

Table S7 The distance between two $FeN_4(OH)$ active sites (d_{Fe-Fe}), two adsorbed *Os (d_{*O-*O}) in different carbon nanotubes together with the corresponding ΔG_5 and overpotentials (η).

	d_{Fe-Fe} (Å)	d_{*O-*O} (Å)	ΔG_5 (eV)	η (V)	
				Single-active-site Mechanism	Dual-active-sites Mechanism
CNT (5, 0)	5.45	1.41	-5.71	≥3.62	5.13
CNT (6, 0)	6.25	1.34	-2.26	≥1.70	3.59
CNT (7, 0)	6.47	2.32	-1.75	≥0.37	1.62
CNT (8, 0)	7.14	2.83	-0.43	0.91	0.18
CNT (9, 0)	7.73	3.56	-0.43	1.00	0.27
CNT (10, 0)	8.51	4.63	--	1.05	--
CNT (11, 0)	9.01	4.85	--	0.90	--
CNT (12, 0)	10.14	5.89	--	0.97	--

References

(1) G. Kresse, J. Furthmuller. *J. Comput. Mater. Sci.* 1996, **6**, 15-50.

(2) J. P. Perdew, K. Burke, M. Ernzerhof. *Phys. Rev. Lett.* 1997, **78**, 1396-1396.

(3) P. E. Blöchl. *Phy. Rev. B* 1994, **50**, 17953-17979.

(4) S. Grimme. *J. Comput.Chem.* 2006, **27**, 1787-1799.

(5) G. Henkelman, B. P. Uberuaga, H. Jónsson. *J. Chem. Phy.* 2000, **113**, 9901-9904.

(6) H. Xu, D. Chen, D. Cao, X. Zeng, *Nat. Catal.*, 2018, **1**, 339-348.